

Cholesterol Modulates the Organization of the γ M4 Transmembrane Domain of the Muscle Nicotinic Acetylcholine Receptor

Rodrigo F. M. de Almeida,* Luís M. S. Loura,*[†] Manuel Prieto,* Anthony Watts,[‡] Aleksandre Fedorov,* and Francisco J. Barrantes[§]

*Centro de Química-Física Molecular, Instituto Superior Técnico, Lisboa, Portugal; [†]Departamento de Química, Universidade de Évora, Évora, Portugal; [‡]Biochemistry Department, Oxford University, Oxford, United Kingdom; and [§]UNESCO Chair of Biophysics & Molecular Neurobiology and Instituto de Investigaciones Bioquímicas de Bahía Blanca, Argentina

ABSTRACT A 28-mer γ M4 peptide, obtained by solid-state synthesis and corresponding to the fourth transmembrane segment of the nicotinic acetylcholine receptor γ -subunit, possesses a single tryptophan residue (Trp⁴⁵³), making it an excellent model for studying peptide-lipid interactions in membranes by fluorescence spectroscopy. The γ M4 peptide was reconstituted with synthetic lipids (vesicles of 1-palmitoyl-2-oleoyl-*sn*-glycero-3-phosphocholine, i.e., POPC) rich and poor in cholesterol and analyzed using steady-state and time-resolved fluorescence techniques. The decrease in γ M4 intrinsic fluorescence lifetime observed upon incorporation into a cholesterol-rich *lo* phase could be rationalized on the basis of a dynamic self-quenching owing to the formation of peptide-rich patches in the membrane. This agrees with the low Förster type resonance energy transfer efficiency from the Trp⁴⁵³ residue to the fluorescent cholesterol analog, dehydroergosterol, in the *lo* phase. In the absence of cholesterol the γ M4 nicotinic acetylcholine receptor peptide is randomly distributed in the POPC bilayer with its hydrophobic moiety matching the membrane thickness, whereas in the presence of cholesterol the increase in the membrane thickness and variation of the material properties favor the formation of peptide-enriched patches, i.e., interhelix interaction energy is essential for obtaining a stabilized structure. Thus, the presence of a cholesterol-rich, ordered POPC phase drives the organization of peptide-enriched patches, in which the γ M4 peptide occupies \sim 30% of the patch area.

INTRODUCTION

The nicotinic acetylcholine receptor (AChR) is one of the best-characterized members of the ligand-gated ion channel superfamily (see reviews in Barrantes, 1998, 2003). It is a pentamer of homologous $\alpha_2\beta\gamma\delta$ subunits. Each subunit contains four hydrophobic segments (M1–M4), which constitute membrane-spanning domains (Blanton and Wang, 1991; Blanton and Cohen, 1992, 1994). The M2 segment from each subunit contributes structurally to form the ion channel proper. The M4 segment is the transmembrane domain more exposed to the bilayer lipid, and the M1 and M3 segments are also in contact with lipid, since they are labeled by membrane-partitioning photoactivatable probes (Blanton and Wang, 1991; Blanton and Cohen, 1992, 1994; Blanton et al., 1999).

Experimental evidence from various groups, including ours, has reinforced the view that the function of the AChR is influenced by its lipid microenvironment (see reviews in Barrantes, 2001, 2003). The exact nature of the interactions between the AChR transmembrane region and the adjacent lipids has not been clearly established. Since the discovery of an immobilized layer of lipids surrounding the AChR (shell, boundary, or annular lipids; Marsh and Barrantes, 1978), this distinct region has been postulated as the likely candidate

where the modulation of the AChR function by lipids occurs. Several hypotheses have been put forward with regard to the biophysical state of the boundary lipids (Fong and McNamee, 1987; Jones and McNamee, 1988) and/or to the existence of distinct sites at the AChR-lipid interface (Jones and McNamee, 1988; Antollini and Barrantes, 1998, 2002; Addona et al., 1998). All hypotheses have in common the occurrence of modulatory effects on AChR function, and both endogenous and exogenous lipids (acting as hydrophobic noncompetitive inhibitors) are postulated to influence the AChR (see, for example, Jones and McNamee, 1988; Rankin et al., 1997; Addona et al., 1998; Baenzinger et al., 2002).

The interaction of cholesterol (Chol) with lipids in general is well described in the literature. For high Chol concentrations, the lipid phase transition disappears and a new single phase called the liquid-ordered phase (*lo*) is formed (Ipsen et al., 1987), with properties in between the gel and the fluid phases. For low Chol concentrations, the phases are called solid-ordered (*so*) or liquid-disordered (*ld*), depending on whether the system is above or below its gel-fluid transition temperature (T_m), respectively. When the binary lipid system is at intermediate Chol concentrations, there is phase coexistence of *so* and *lo* (below), or of *ld* and *lo* (above), depending on the temperature relative to T_m .

The possible modulation of AChR structure and/or function by sterols was postulated in early experimental work in which the presence of sterols in the receptor-vicinal lipid was demonstrated (Marsh and Barrantes, 1978; Marsh et al., 1981). Labeling and tryptic digestion studies have demonstrated that the α M1, α M4, and γ M4 transmembrane segments of the AChR interact with Chol (Corbin et al.,

Submitted August 12, 2003, and accepted for publication December 15, 2003.

Address reprint requests to Francisco J. Barrantes, UNESCO Chair of Biophysics & Molecular Neurobiology and Instituto de Investigaciones Bioquímicas de Bahía Blanca, C.C. 857, Camino La Carrindanga km 7, B8000FWB, Argentina. E-mail: rtfjb1@criba.edu.ar.

© 2004 by the Biophysical Society

0006-3495/04/04/2261/12 \$2.00

1998), and photoaffinity sterol reagents like the promegestol promegestone, label the AChR transmembrane domains (Blanton et al., 1999). Fluorescence spectroscopy studies have shown different degrees of selectivity of other steroids like cholestane and androstane spin labels for the purified, reconstituted AChR and for transmembrane peptides α M4, γ M4, α M1, and γ M1 (Barrantes et al., 2000).

In this work, the AChR γ M4 transmembrane peptide was reconstituted in membrane model systems (vesicles of 1-palmitoyl-2-oleoyl-*sn*-glycero-3-phosphocholine—that is, POPC—and Chol) and studied using fluorescence techniques by following the spectral and photophysical properties in steady and transient states. Changes in peptide fluorescence lifetime, dynamic self-quenching, Förster-type fluorescence resonance energy transfer (FRET) efficiency measurements from the peptide (Trp residue) to the fluorescent Chol analog, dehydroergosterol (DHE), are used to study the influence of Chol on γ M4 peptide distribution. In the absence of Chol the AChR peptide is randomly distributed in the bilayer, whereas in the presence of Chol a nonrandom distribution of the peptide is apparent in POPC membranes in the *lo* phase, even at low peptide concentrations. This probably results from the combined effects of increased membrane thickness and changes in material properties (Lundbaek et al., 2003), which favors the peptide aggregation, i.e., the interhelix interaction energy is essential for obtaining a stabilized structure. Therefore, Chol drives the system (i.e., the transmembrane segments) to a superstructure that may bear relevance to the assembly processes leading to the organization of the transmembrane bundles in the whole AChR.

MATERIALS AND METHODS

Chemicals

A peptide corresponding to the AChR transmembrane segment γ M4 and the two extramembranous regions, and having the sequence *n*-Asp-Lys-Ala-Cys-Phe-Trp-Ile-(²H₃)Ala-Leu-Leu-(1-¹³C)Leu-Phe-Ser-Ile-(¹⁵N)Gly-Thr-Leu-Ala-Ile-Phe-Leu-Thr-(2-¹³C)Gly-His-Phe-Asn-Gln-Val-C, was prepared using conventional Fmoc synthesis (NSR Centrum, Nijmegen, Holland). All labeled amino acids were purchased from Cambridge Isotopes (Andover, MA) and protected using conventional Fmoc chemistry. The resulting peptide was deemed to be >90% pure as determined by analytical HPLC and mass spectrometry. γ M4 was kept lyophilized at -80°C until use. The lipid 1-palmitoyl-2-oleoyl-*sn*-glycero-3-phosphocholine (POPC) was purchased from Avanti Polar Lipids (Birmingham, AL). Chol and dehydroergosterol (DHE) were from Sigma (St. Louis, MO). *trans*-parinaric acid (*t*-PnA) and *tris*(2-cyanoethyl)phosphine (TCP) were obtained from Molecular Probes (Eugene, OR). Roche Diagnostics (Mannheim, Germany) supplied a kit for Chol determination. All other reagents were of the highest purity available. All materials were used without further purification.

Liposome preparation

Adequate amounts of stock solutions of host lipids, peptide, and probes (except *t*-PnA) were mixed in a chloroform/methanol solution, dried under a stream of nitrogen, and suspended in buffer (20 mM HEPES, 10 mM NaCl, 0.1 mM EDTA, pH = 7.4) to obtain multilamellar vesicles (MLV). The small unilamellar vesicles (SUV) used in this study were obtained after

power sonication (Branson Sonifier model 250, 40 W; Branson Ultrasonics, Danbury, CT). Total γ M4 peptide concentration varied between 10 and 20 μ M. The lipid concentration was varied according to peptide concentration; for 7% peptide, the final lipid concentration was 0.3 mM; for 3% peptide, lipid concentration was 0.5 mM; for 0.7% peptide, lipid concentration was 1.2 mM. These concentrations were used for the time-resolved self-quenching study, where the only relevant parameter is the lipid/peptide ratio. All-monomer peptide samples were obtained by reduction of the disulfide bridge along with sonication using the 1/8" microtip in a Branson Sonifier model 250 or by incubation with the reducing agent TCP. For the FRET experiments a total lipid (SUV of POPC and Chol) concentration of 1 mM was used, of which 40 mol % corresponded to Chol. The peptide concentration (donor) was kept constant (1 mol %) and its concentration was determined from the absorption spectrum ($\epsilon = 5690 \text{ M}^{-1} \text{ cm}^{-1}$ at $\lambda = 280 \text{ nm}$, Gill and von Hippel, 1989). The acceptor (DHE) concentration varied up to 4 mol % by replacing Chol. DHE concentrations were determined from absorption measurements ($\epsilon = 11,200 \text{ M}^{-1} \text{ cm}^{-1}$ at $\lambda = 328 \text{ nm}$ in chloroform; Smutzer et al., 1986; $\epsilon = 9500 \text{ M}^{-1} \text{ cm}^{-1}$ at $\lambda = 328 \text{ nm}$ in membranes, this article).

In the time-resolved fluorescence self-quenching study, the peptide concentration was varied between 0.7 and 7% (*ld*, effect of peptide concentration) or kept at 0.7 mol % (effect of *ld* versus *lo* phase fraction) and the experiments were carried out using MLV. In the latter case, *t*-PnA (0.33 mol %) was used in the presence and absence of peptide to evaluate the eventual perturbation induced by the peptide on the POPC/Chol phase diagram and to calibrate the liquid-ordered (*lo*) mole fraction. Its concentration in the membrane was evaluated from absorption spectroscopy ($\epsilon = 89,000 \text{ M}^{-1} \text{ cm}^{-1}$ at $\lambda = 299.4 \text{ nm}$ in ethanol; Sklar et al., 1977). *t*-PnA was added to the vesicles from an ethanol concentrated solution to minimize the volume of ethanol added to the vesicle suspension (keeping this value <1%, the membrane bilayer structure is not affected (Vierl et al., 1994). This injection method for introduction of the probe enables one to conduct the photophysical measurements on the peptide, and subsequently the *t*-PnA fluorescence decay studies, on the very same samples. Before the photophysical measurements, the vesicle suspensions were degassed by bubbling nitrogen to prevent photo-oxidation of the unsaturated compounds.

Absorption and fluorescence measurements

Absorption spectra were obtained in a Shimadzu UV-3101PC spectrophotometer (Shimadzu Schweiz, Reinach, Switzerland) using spectral bandwidths of 2.0 nm. The correction for light scattering was carried out according to a reported methodology (Castanho et al., 1997). Steady-state fluorescence spectra were obtained in an SLM-Aminco 8100 Series 2 spectrofluorimeter (Jobin Yvon, Edison, NJ). Emission spectra were corrected using standard emission spectra of L-Tyr and L-Trp (Chen, 1967); 5 mm \times 5 mm quartz cuvettes and spectral bandwidth of 2–8 nm were used.

The time-resolved instrumentation (single-photon timing technique) was previously described (Loura et al., 1996). Trp emission (excitation at $\lambda = 288 \text{ nm}$) was measured at $\lambda = 340 \text{ nm}$ using the magic angle (54.7°) relative to the vertically polarized excitation beam. The fluorescence decays of the γ M4 peptide were obtained with an accumulation of 20,000 counts in the peak channel and timescales ranging from 22 ps/channel (*ld*, 0.7 mol %) to 15.3 ps/channel (*lo* or *ld*, higher peptide concentrations). The *t*-PnA decays were obtained with excitation at $\lambda = 303 \text{ nm}$, its emission being collected at $\lambda = 406 \text{ nm}$, with 20,000 maximum counts, and timescales between 30.6 ps/channel (*ld*) and 56.7 ps/channel (*lo*). For the FRET experiments, excitation was at $\lambda = 284 \text{ nm}$ to minimize DHE absorption, and for the emission at $\lambda = 310 \text{ nm}$ an interference filter was added to the monochromator to avoid scattered excitation light and acceptor emission. The number of counts on the peak channel was 7000, and a timescale of 11 ps/channel was used. Data analysis was carried out using a nonlinear, least-squares iterative convolution method based on the algorithm of Marquardt (1963). The goodness of the fit was judged from the reduced χ^2 , weighted residuals, and autocorrelation plots.

The average lifetime $\bar{\tau}$ of a fluorophore with a complex fluorescence decay described by a sum of exponentials as

$$i(t) = \sum_i a_i \exp(-t/\tau_i), \quad (1)$$

and is defined as in Lakowicz (1999),

$$\bar{\tau} = \frac{\sum_i a_i \tau_i^2}{\sum_i a_i \tau_i}, \quad (2)$$

where a_i are the normalized pre-exponentials (amplitudes) and τ_i are the lifetime components.

The lifetime-weighted quantum yield $\langle\tau\rangle$ is described following Lakowicz (1999) as

$$\langle\tau\rangle = \frac{\sum_i a_i \tau_i}{\sum_i a_i}. \quad (3)$$

The critical distance for energy transfer, R_0 , was calculated from Eq. 4 (Berberan-Santos and Prieto, 1987),

$$R_0 = 0.2108 \times \left[\kappa^2 \times \Phi_D \times n^{-4} \times \int_0^\infty I(\lambda) \times \varepsilon(\lambda) \times \lambda^4 d\lambda \right]^{1/6}, \quad (4)$$

where κ^2 is the orientation factor, Φ_D is the donor quantum yield in the absence of acceptor, n is the refractive index, $I(\lambda)$ is the normalized donor emission spectrum, and $\varepsilon(\lambda)$ is the acceptor molar absorption spectrum (expressed as $M^{-1} \text{ cm}^{-1}$). If the λ units used in Eq. 4 are nm, then the calculated R_0 has Å units.

Energy transfer efficiencies, E , were experimentally determined from

$$E = 1 - \langle\tau\rangle_{\text{DA}} / \langle\tau\rangle_{\text{D}}, \quad (5)$$

where $\langle\tau\rangle_{\text{DA}}$ and $\langle\tau\rangle_{\text{D}}$ are the lifetime-weighted quantum yields of the donor in the presence and absence of acceptor, respectively.

The steady-state anisotropies, $\langle r \rangle$, were determined according to Lakowicz (1999), as

$$\langle r \rangle = \frac{I_{\text{VV}} - GI_{\text{VH}}}{I_{\text{VV}} + 2GI_{\text{VH}}}, \quad (6)$$

where I_{ij} are the steady-state vertical and horizontal components of the fluorescence emission with excitation vertical (I_{VV} and I_{VH}) and horizontal (I_{HV} and I_{HH}) to the emission axis. The correction for orientation-dependent transmittance of the emission polarizer was determined using horizontally polarized excitation light to calculate the G factor ($G = I_{\text{HV}}/I_{\text{HH}}$). Polarization measurements were made using quartz Gian-Thompson prism polarizers in a single-channel detection system and an adequate blank was subtracted from each intensity reading before the calculation of the anisotropy value.

For fluorophores with hindered rotation, the time-resolved anisotropy does not decay to zero and tends to a limiting value r_∞ instead. This value can be obtained from the vertical and horizontal components of the fluorescence decay, and no deconvolution methods are required because the laser excitation pulse has no influence on the decay at long times.

Other analytical procedures

Lipid concentration was determined by inorganic phosphorus analysis (McClare, 1971), and for Chol determination an enzymatic method was

used. In this method, the reaction of Chol with oxygen is first catalyzed by Chol oxidase, to produce hydrogen peroxide. Peroxidase is subsequently used to catalyze the reaction of hydrogen peroxide with 4-aminophenazone and phenol, producing 4-(*p*-benzoquinone-monoimino)-phenazone, which is a colored compound (Deeg and Ziegenhorn, 1983). Absorbance (proportional to Chol concentration) is measured at 500 nm.

RESULTS

Trp photophysics and fluorescence self-quenching

Because of the existence of a cysteine residue in γM4 (Cys⁴⁵¹), in the absence of reducing agents the peptide occurs as a mixture of monomeric and dimeric (disulfide bonded) forms, but predominantly as a monomer (data not shown). The fluorescence of the γM4 peptide incorporated in liposomes made of 60% POPC/40% Chol MLV is shown in Fig. 1. The spectral position (not shown) and the steady-state anisotropy, $\langle r \rangle$ (Table 1), are insensitive to the presence of Chol, i.e., they are the same in *ld* and *lo* phases, and the anisotropies are reasonably high and typical of a Trp-containing peptide strongly immobilized in a membrane. The emission maximum of γM4 Trp⁴⁵³ in POPC MLV has a maximum at $\lambda = 325$ nm (Fig. 1). The significant blue-shift relative to an aqueous environment ($\Delta\lambda = 25$ nm) clearly shows that Trp⁴⁵³, although near the interface (see below), is essentially in a nonsolvating environment. The absence of peptide in the aqueous solution (also corroborated from its absence in the supernatant after centrifugation of the vesicles) is not surprising, because γM4 is a rather hydrophobic transmembrane peptide, presumably with an α -helical structure (Barrantes et al., 2000; Miyazawa et al., 2003). Using the parallax method, Chattopadhyay and McNamee (1991) showed that the membrane-embedded Trp⁴⁵³ residue in purified *Torpedo californica* AChR in DOPC lies ~ 10.1 Å from the center of the bilayer (5 Å from the lipid polar headgroup region). From differential quenching experiments of pyrene-labeled Cys⁴⁵¹, it was reported that this residue is located at a shallow position in the bilayer, near the membrane-water interface (Barrantes

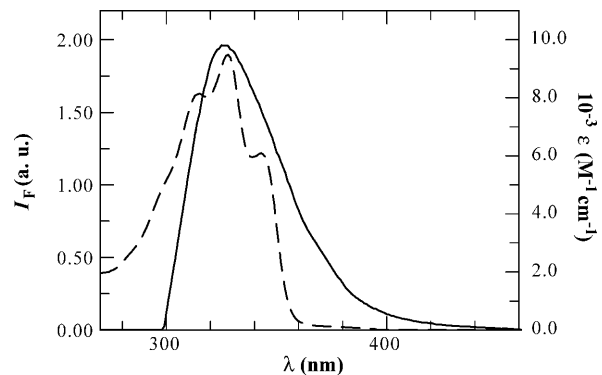


FIGURE 1 Emission spectrum of γM4 ($\lambda_{\text{exc}} = 288$ nm) in POPC vesicles (solid line) and absorption spectrum of DHE in POPC/Chol (3:2) vesicles (dashed line) at room temperature.

TABLE 1 Photophysical properties of the Trp⁴⁵³ residue in the γ M4 peptide incorporated into POPC/Chol vesicles with low (*ld* phase) or high (*lo* phase) Chol content at room temperature

γ M4 (mol %)	$\langle\tau\rangle_{ld}$ (ns)	$\langle\tau\rangle_{lo}$ (ns)	$\bar{\tau}_{ld}$ (ns)	$\bar{\tau}_{lo}$ (ns)	$\langle r \rangle_{ld}$	$\langle r \rangle_{lo}$
0.7	3.04 \pm 0.05	1.47 \pm 0.10	4.29	2.84	0.089 \pm 0.006	0.091 \pm 0.012
3.0	2.11 \pm 0.08	1.44 \pm 0.11	3.53	2.69	0.078 \pm 0.007	0.076 \pm 0.006
7.0	1.43 \pm 0.08	—	2.81	—	0.080 \pm 0.008	—

$\lambda_{exc} = 288$ nm and $\lambda_{em} = 340$ nm. The concentration of γ M4 peptide is expressed in mol % relative to total lipid. See text for further details.

et al., 2000). It can therefore be concluded that Trp⁴⁵³, only ~ 3 Å further into the membrane core from Cys⁴⁵¹, is also near the interface, probably very near the carbonyl/first carbons of the acyl chain region of the phospholipid bilayer, as recently depicted by Miyazawa et al. (2003). This is in fact the most common behavior of Trp residues in membrane proteins (Ridder et al., 2000).

The fluorescence decays of Trp could be described by a sum of three exponentials (reduced $\chi^2 < 1.3$). The lifetime-weighted quantum yields, $\langle\tau\rangle$, both for the *ld* and *lo* phases, are shown in Table 1 for several γ M4 peptide concentrations. In the *ld* phase, upon increasing the concentration from 0.7 mol % up to 7 mol %, the Trp lifetime-weighted quantum yield was reduced to one-half (Table 1). This can be accounted for by the presence of Cys and Lys residues in the γ M4 transmembrane domain, which are known to be efficient quenchers of Trp fluorescence (Chen and Barkley, 1998). Thus, at higher concentrations the proximity between γ M4 peptides leads to the diminution of the Trp intrinsic fluorescence due to an intermolecular self-quenching process. It should be stressed that all the intramolecular quenching effects are taken into account in the fluorescence lifetime without intermolecular quenching, which is the case for the diluted peptide in *ld* vesicles.

For the *lo* phase, the lifetimes do not show such a strong variation, and in addition, the values for the lower concentrations (0.7% and 3%) in *lo* are close to those found for the higher concentrations in *ld* (7%). Also, as the dynamic self-quenching mechanism depends on the quencher concentration sensed by the fluorophore, in the case of γ M4 in Chol-rich vesicles, a higher effective peptide concentration occurs, augmenting the extent of the self-quenching process.

Because the occurrence of an intermolecular self-quenching process is clearly observed in the case of a single phase, it is possible to exploit this phenomenon to study the effect of Chol concentration on the organization of the γ M4 peptide. The dependence of fluorescence lifetime of γ M4 on *lo* phase mole fraction (proportional to Chol concentration within the *ld/lo* phase coexistence range) is shown in Fig. 2, where $\langle\tau\rangle$ of the peptide, now at a constant concentration (0.7 mol %), is shown to decrease upon increasing the Chol concentration. It should be stressed that the data is plotted versus the mole fraction of *lo* phase within the *ld/lo* phase coexistence range (along a tie-line). This was obtained from the phase diagram of this lipid-Chol mixture, as described in the literature (e.g., Mateo et al., 1995) or from our own data (de Almeida et al.,

2003). For POPC/Chol mixtures at 20°C and between ~ 0.05 and ~ 0.40 Chol mole fraction, there is a broad phase coexistence range of *ld* and *lo* phases.

Because it could be speculated that the presence of the peptide might disturb the POPC/Chol phase diagram by, for example, some ordering or disordering effect, the *t*-PnA fluorescence lifetime was measured in the absence and presence of the peptide (Fig. 3). The *t*-PnA fluorescence lifetime was described by the sum of three exponentials with components close to reported values (Mateo et al., 1995), which were obtained following a different analytical methodology—the maximum entropy method. The phase boundaries are essentially the same as the ones reported in the literature for this lipid mixture. Because it is not affected by the peptide, the value of *t*-PnA partition constant between the *lo* and *ld* phases ($K_p^{(lo/ld)} = 0.8$) was used to calibrate the Chol concentrations, i.e., the lifetime-weighted quantum yields were used to calculate the *lo* fractions (Figs. 2 and 3) using formalisms previously published (de Almeida et al., 2002).

FRET from γ M4 (Trp⁴⁵³) to dehydroergosterol (DHE)

To obtain information on the affinity of the γ M4 peptide for Chol, FRET measurements were carried out using Trp⁴⁵³ and the fluorescent Chol analog DHE as donor and acceptor, respectively. In this series of experiments the totally reduced all-monomer species of γ M4 was used, since the presence of

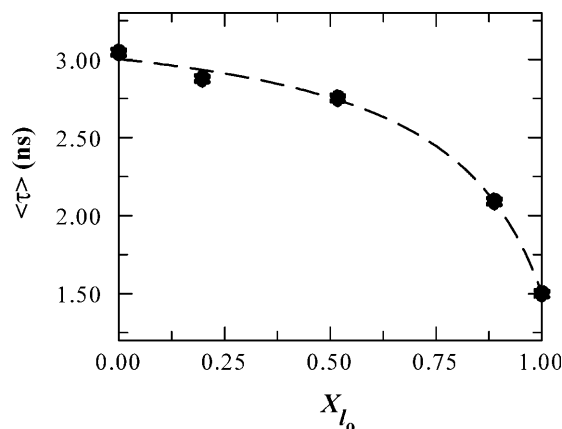


FIGURE 2 Lifetime-weighted fluorescence quantum yield of γ M4 Trp residue versus the molar fraction of *lo* phase. The peptide is 0.7 mol % of the total lipid. The line is merely a guide to the eye.

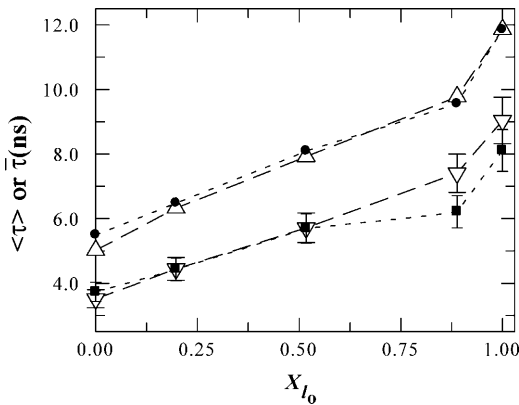


FIGURE 3 *t*-PnA (0.33 mol % of total lipid) mean fluorescence lifetime (Δ , \bullet) and lifetime-weighted quantum yield (∇ , \blacksquare) in the absence (∇ , Δ) and presence (\bullet , \blacksquare) of the γ M4 peptide (0.7 mol %) incorporated in POPC/Chol vesicles with compositions spanning the *lo*/*ld* phase coexistence range. The lines are guides to the eye.

dimer would introduce an additional complexity into the analysis of FRET data: two Trp donors would be present in the dimer, the system topology would lose cylindrical symmetry around each donor (see Discussion), and a complex geometry regarding the excluded volume for transfer would have to be considered. To further reduce the complexity of the system, the monomeric γ M4 species was reconstituted in SUV to avoid a multilayer geometry and to minimize light scattering data biasing. Another important advantage of SUV relative to larger model membranes is the absence of DHE tail-to-tail dimerization that is observed in 100-nm diameter vesicles (Loura and Prieto, 1997) and which would also render the analysis of the FRET results more difficult. Evidence for the reduction of the disulfide bridge of γ M4 upon sonication, as previously observed for other peptides (Santos et al., 1998), was obtained from the very small steady-state intensities (not shown) with maintenance of the lifetime-weighted quantum yield (see below). In this case, there is a strong, very effective intramolecular static quenching due to the nearby $-\text{SH}$ group. Identical fluorescence behavior was obtained upon incubation with the reducing agent TCP. Although the parameters recovered from the fit to the experimental decays were essentially the same, the reduced χ^2 of the fit was higher in the presence of TCP, and therefore no chemical quenching agent was employed in subsequent experiments.

The Förster radius was calculated next from the experimental data in Fig. 1—the donor's emission (Trp⁴⁵³) and the acceptor's (DHE) absorption. Values of $\kappa^2 = 2/3$ (dynamic isotropic limit; see Van Der Meer et al., 1994 for a detailed discussion), and $n = 1.44$ (Davenport et al., 1985) were considered in Eq. 4. The fluorescence quantum yield $\Phi_D = 0.067$ was estimated on the basis of the Trp lifetime-weighted quantum yield as compared to that of *n*-acetyltryptophanamide, a well-known model for this amino acid residue within a polypeptide chain (Szabo and

Rayner, 1980). This procedure avoids all the errors related to the determination of quantum yields in scattering media using steady-state data, and it does not take into account effects of static quenching by sulfhydryl groups. A value of $R_0 = 20 \text{ \AA}$ was obtained from the spectral overlap of Trp⁴⁵³ emission and DHE absorption shown in Fig. 1.

The fluorescence decay of Trp⁴⁵³ is described by a sum of three exponentials, and for the determination of FRET efficiency, E (Eq. 5), decay integration was carried out to determine the lifetime-weighted quantum yields, $\langle \tau \rangle$. It should be pointed out that this study could not be carried out using steady-state techniques due to the strong absorption overlap of donor and acceptor, leading to large inner filter effects, and the low steady-state intensities for the reduced species, preventing the measurement of reliable absolute intensities. The variation of E upon increasing acceptor concentration is shown in Fig. 4. FRET efficiency was found to be lower than that expected on the basis of a random distribution.

DISCUSSION

In the present work we have exploited the single Trp (Trp⁴⁵³) intrinsic fluorescence of a 28-mer synthetic peptide analog of the γ M4 reconstituted in POPC vesicles, rich and poor in Chol, to learn about the structure of the peptide and about the possible effects of the sterol on peptide distribution in the membrane.

Studies by Blanton and co-workers (Blanton and Cohen, 1992, 1994; Blanton et al., 1999), using hydrophobic photoactivatable probes made apparent a periodicity of the tagged lipid-exposed residues in M4 and M3, which is fully consistent with an α -helical structure. Deuterium-exchange

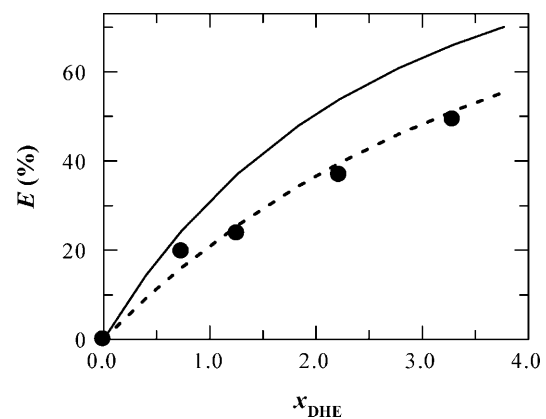


FIGURE 4 FRET efficiency from γ M4 Trp⁴⁵³ (totally reduced monomeric species) to DHE ($R_0 = 20 \text{ \AA}$) versus acceptor mol fraction. The circles are experimental data points. The solid line is the calculated FRET efficiency for a random distribution of acceptors in the plane of the membrane with an exclusion radius of 5 \AA , to account for the area occupied by the α -helix donor. Both in-plane and out-of-plane (interplanar distance of 22 \AA) FRET are considered. See text for further details on the calculations. The dotted line is also based on a random distribution model considering only 62% DHE molecules available as acceptors.

Fourier transform infrared studies also indicated a predominantly α -helical structure in other AChR membrane-embedded domains (e.g., Méthot et al., 2001). Very recent cryoelectron microscopy data (Miyazawa et al., 2003) appear to confirm the biochemical studies, and suggest that all AChR TM peptides are helical, and adopt the antiparallel α -helical bundle motif. Fluorescence studies of pyrene-labeled Cys residues in reconstituted intact AChR and receptor-derived peptides appear to validate the use of the latter as faithful models, and in the particular case of γ M4 indicate that this segment is a straight α -helix (Barrantes et al., 2000).

Learning about γ M4 structure from energy homotransfer and anisotropy studies

In the absence of a reducing agent, and because there is a cysteine residue in the peptide sequence, γ M4 has the ability to form dimers, although the monomeric species predominates (data not shown). The dimer has two Trp⁴⁵³ residues, one in each helix, which can lead to energy homotransfer (energy migration) between these two Trp residues. This interaction can be used to obtain structural information (distances) on the peptide. As a consequence of energy migration, Trp anisotropy may decrease. The expected value for the dimer anisotropy $\langle r \rangle_D$ can be determined following Runnels and Scarlata (1995), as

$$\langle r \rangle_D = \langle r \rangle_M (1 + (R_0/l)^6) / (1 + 2(R_0/l)^6) + \langle r \rangle_{ET} (R_0/l)^6 / (1 + 2(R_0/l)^6), \quad (7)$$

where l is the distance between the two chromophores, R_0 is the Förster radius for energy migration, $\langle r \rangle_M$ is the anisotropy of the initially excited molecule, and $\langle r \rangle_{ET}$ is the anisotropy of the second molecule of the pair. This second contribution can be disregarded because it is smaller than 4% of the first one at all times (Berberan-Santos and Valeur, 1991). To obtain the inter-Trp distance, we fed the experimentally determined value of $\langle r \rangle_D$ for the dimer into Eq. 7. In the energy heterotransfer experiments described in the Results section, the reduced species, i.e., the monomer, was used. However, the monomer anisotropy $\langle r \rangle_M$ could not be evaluated because of the strong fluorescence quenching produced by the $-SH$ group in Cys⁴⁵¹. This fact also rules out any biasing of steady-state anisotropy data, due to the presence of residual dimeric species. The steady-state intensity was too low to yield reliable data. We therefore resorted to literature values from a systematic study of time-resolved anisotropy in which Trp were introduced in different positions along an α -helical peptide in a fluid membrane (Vogel et al., 1988). Trp residues located near the surface, such as Trp-1, or at a shallow position in the hydrocarbon core, such as Trp-6 in the cited work (a condition identical to that of the γ M4 peptide under study), constitute a suitable model to obtain $\langle r \rangle_M$.

We calculated the steady-state value by integration of the reported time-resolved data of Vogel et al. (1988) according to Eqs. 1 and 8,

$$r(t) = (r_0 - r_\infty) \sum_i \beta_i \exp(-t/\theta_i) + r_\infty, \quad (8)$$

where r_0 is the fundamental anisotropy, r_∞ is the limiting anisotropy, θ_i are the rotational correlation times, and β_i are the associated fractions for each θ_i .

The steady-state anisotropy results from

$$\langle r \rangle = \int_0^\infty i(t)r(t) dt / \int_0^\infty i(t) dt. \quad (9)$$

In Eq. 9, both the lifetime data of Vogel et al. (1988) and our own were used, leading in both cases to an identical value for the anisotropy: $\langle r \rangle_M = 0.082 \pm 0.013$, which is not significantly different from that obtained for the dimeric peptide in the present study (Table 1). It can therefore be concluded that there is no relevant energy migration in the dimer, allowing us to set a lower boundary for the inter-Trp distance.

A Förster radius $R_0 = 10 \text{ \AA}$ for energy migration was calculated according to Eq. 4 considering $\Phi_D = 0.13$. This value was obtained again by comparing the lifetime-weighted quantum yields of the γ M4 peptide and that of *n*-acetyltryptophanamide. From Eq. 7 it is predicted that for interchromophore distances $\lesssim 2R_0$, the degree of depolarization as a consequence of energy migration is insignificant. This corresponds to a distance of 20 \AA in the present case. In fact, for two helices connected by a disulfide bond, each Trp residue would be in an approximately diametrically opposed position, because for an ideal α -helix, an arc of $\sim 200^\circ$ would be subtended between Trp⁴⁵³ and Cys⁴⁵¹ (Fig. 5 A).

Learning about γ M4 lateral distribution from fluorescence self-quenching

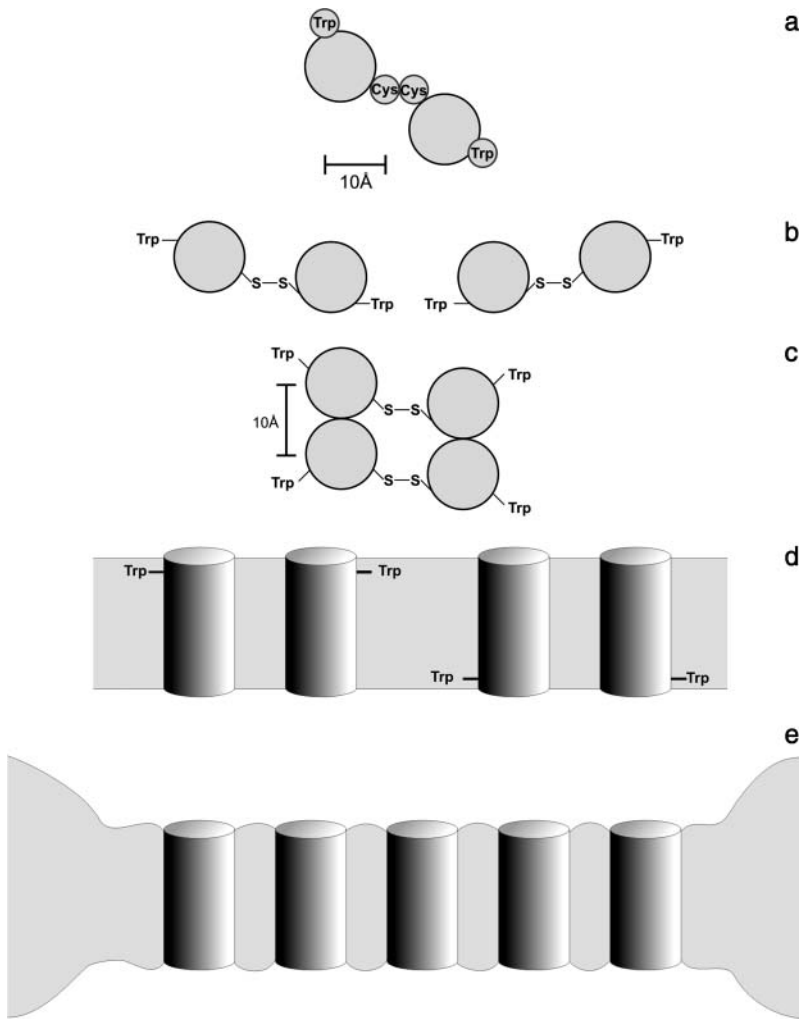
The effects of the collisional contribution of self-quenching on the fluorescence lifetime for a molecule with a complex decay are described by the Stern-Volmer equation (Sillen and Engelborghs, 1998), as

$$\langle \tau \rangle_0 / \langle \tau \rangle = 1 + \langle k_q \rangle \times \bar{\tau}_{0q} [F], \quad (10)$$

where $\bar{\tau}_{0q}$ is given by

$$\bar{\tau}_{0q} = \sum_i a_{0i} \tau_i \tau_{0i} / \sum_i a_{0i} \tau_i. \quad (11)$$

The subscript 0 indicates the absence of quencher (in our case, the values for the sample with the lowest peptide concentration), $\langle k_q \rangle$ is the bimolecular quenching rate constant, the brackets indicate that this is a (complex) average of



a

b

c

d

e

FIGURE 5 Putative organization of γ M4 in Chol-poor and Chol-rich systems. A plausible structural framework to account for the absence of energy migration between Trp⁴⁵³ residues in the γ M4 peptide, and the variation of lifetime-weighted quantum yield with peptide concentration on the *ld* and *lo* phases, is provided. (a) Top view of the α -helical peptide showing the relative positions of Trp⁴⁵³ and Cys⁴⁵¹, and a probable geometry for a disulfide-bonded dimer. (b) Possible geometry for a linear aggregate. This structure is ruled out. (c) Parallel aggregate in end-on view. This structure is not ruled out by energy homotransfer data. (d) Antiparallel aggregate, lateral view. This structure is not ruled out by energy homotransfer data. (e) Peptide-rich patch. The model depicts the distribution of γ M4 in POPC/Chol vesicles with high Chol content (*lo* phase). The negative mismatch causes a bilayer deformation in the vicinity of a peptide molecule, and other peptides accommodate better in a region close to where other peptides localize. In the *ld* (Chol-poor phase) the peptide is randomly distributed due to the very good matching between the hydrophobic thickness of the bilayer and the peptide.

the rate constants related to each component of the decay, and $[F]$ is the concentration of the fluorophore. The bimolecular quenching rate constant $\langle k_q \rangle$ is related to the diffusion coefficient of the fluorophore (D) via the Smoluchowski equation (Lakowicz, 1999), taking into account transient effects (Umberger and Lamer, 1945),

$$\langle k_q \rangle = 4\pi N_A (2R_c) (2D) [1 + 2R_c / (2\bar{\tau}_{0q} D)]^{1/2}, \quad (12)$$

where N_A is the Avogadro constant and R_c is the collisional radius.

This equation assumes diffusion in an isotropic three-dimensional medium. If the membrane were strictly bi-dimensional, different boundary conditions for the Smoluchowski formalism could be applied (Razi-Naqvi, 1974). The best approach to the specific situation of probe diffusion in a membrane is the one used by Owen (1975), in which the finite bilayer width (cylindrical geometry) is taken into account. Owen introduced the parameter τ_s , which defines the transition from the spherical (three-dimensional) to the

cylindrical geometry, its value being $\tau_s = 16$ ns when considering the bilayer (Wiener and White, 1992) and the peptide/Trp (Zamyatin, 1972) parameterization. This value of τ_s is much longer than the longest fluorescence lifetime of Trp⁴⁵³ in the γ M4 peptide (~ 5 ns), and longer than our experimental time-window (15.3 ns = 15.3 ps/channel \times 1000 channels); the three-dimensional framework approximation is therefore essentially correct. If we consider that the lifetime-weighted quantum yield of the more diluted γ M4 peptide concentration is the limiting $\langle \tau \rangle_0$ (no quenching occurring) (Table 1), a value of $\langle k_q \rangle = 2.6 \times 10^9$ mol⁻¹ dm³ s⁻¹ is obtained from Eq. 10 for the 7 mol % peptide concentration. This value assumes a random peptide analytical concentration in the lipid $[F] = 0.083$ M, determined on the basis of its 7 mol % concentration and considering a volume for the POPC molecule of 1263 Å³ (Small, 1986). A similar value ($\langle k_q \rangle = 2.8 \times 10^9$ mol⁻¹ dm³ s⁻¹) could be obtained for the other peptide concentration, 3%.

If in Eq. 12 we assume the collisional radius for the dimer as 10 Å, diffusion coefficients of $D = 14 \times 10^{-8}$ cm² s⁻¹ (for 7% peptide) and $D = 12 \times 10^{-8}$ cm² s⁻¹ (for 3%

peptide) are obtained. These values have the same order of magnitude or are slightly higher than those typically found for diffusion in an *ld* phase ($D = 1.1 \times 10^{-8} \text{ cm}^2 \text{ s}^{-1}$ (Dietrich et al., 2001), $D = 1\text{--}3 \times 10^{-8} \text{ cm}^2 \text{ s}^{-1}$ for transmembrane proteins and $D = 9\text{--}14 \times 10^{-8} \text{ cm}^2 \text{ s}^{-1}$ for a fluorescent lipid derivative (Vaz et al., 1982) and the fluorescent lipid analog NBD-phosphatidylethanolamine $D = 8 \times 10^{-8} \text{ cm}^2 \text{ s}^{-1}$ (Criado et al., 1982)). Although this is a comparison with values obtained from fluorescence recovery after photobleaching studies of large proteins or from phospholipid single particle tracking studies, the agreement is reasonably good within the framework of the approximations used. This means that the peptide does not appear to exhibit significant aggregation in the *ld* phase. It is also interesting to compare the behavior of the γM4 peptide with the lateral diffusion of the AChR reconstituted in pure dimyristoyl-phosphatidylcholine bilayers and studied with fluorescence recovery after photobleaching techniques. The whole receptor exhibited D -values in the range of $10^{-8} \text{ cm}^2 \text{ s}^{-1}$ for both the AChR monomer and dimer in the liquid-crystalline phase (Criado et al., 1982). Additional multiple-component recoveries with D -values of $<5 \times 10^{-11} \text{ cm}^2 \text{ s}^{-1}$ were found below the lipid phase transition. Thus the translational diffusion of the γM4 peptide is not significantly different from that of the 9S AChR monomer or the 13S dimer in the low concentration limit; neither the peptide nor the whole AChR encounter hindrance to lateral diffusion on the part of the lipid bilayer itself, whereas in native membranes, the densely packed AChR molecules are almost totally immobile (see review in Barrantes, 2001).

However, in the series of experiments in which the peptide concentration was kept constant, a clear decrease of $\langle\tau\rangle$ was observed upon increasing the Chol content in the membrane (Fig. 2). Several explanations for this behavior can be discarded: 1) the phase diagram of the POPC/Chol system is not altered by the presence of peptide (Fig. 3), i.e., the peptide at 0.7 mol% concentration does not disturb the long-range membrane properties; 2), Chol is not a quencher of Trp fluorescence; and 3), despite the same order of magnitude, the diffusion coefficient is lower for the *lo* phase than for the *ld* phase (e.g., a threefold decrease is reported by Dietrich et al., 2001). This slower dynamics does not lead, therefore, to higher quenching. As previously described, self-quenching was observed for a single phase (it is known that several amino acid side chains are effective quenchers of Trp fluorescence), and therefore only a higher effective peptide concentration can be invoked to rationalize the data in Fig. 2. This means that the peptide is not randomly distributed in the *lo* phase and that patches with a higher local concentration of γM4 are formed. Within the framework of a Stern-Volmer analysis (Eq. 10), this higher peptide concentration gives rise to a higher decrease in lifetime. It is interesting to note that in pure *lo* phase, for the lower peptide concentration studied, the lifetime is already quite low (Table 1) and similar to the value for the highest concentration in *ld* phase. It can

therefore be concluded that the formation of γM4 peptide-rich patches is strongly induced by Chol.

Interpeptide energy migration

Since intramolecular energy migration could be discarded, the reasons why anisotropy is largely concentration-independent (Table 1), i.e., the lack of efficient intermolecular energy migration in either the *ld* or *lo* phases, should be discussed.

Before this analysis, the decrease in fluorescence lifetime due to the intermolecular collisional self-quenching must be considered. It should be stressed that energy migration does not affect the lifetime or intensities, i.e., there is no quenching (Valeur, 2001) and only anisotropy decreases. However, the decrease in lifetime by some other mechanism results in an increase in anisotropy (Lakowicz, 1999). Thus the decrease in anisotropy due to energy migration would be hidden due to a compensatory reduction in fluorescence lifetime.

From the Weber law of additivity of anisotropies, the following composition of Perrin equations (considering a complex fluorescence decay, single rotational correlation time, and a single finite value for the limiting anisotropy, r_∞), was obtained, as

$$\langle r \rangle = \frac{r_0 - r_\infty}{\langle \tau \rangle} \sum_i \frac{a_i}{1/\tau_i + 1/\theta} + r_\infty. \quad (13)$$

A value of limiting anisotropy $r_\infty = 0.066$ was experimentally obtained. Considering $r_0 = 0.173$ for excitation at $\lambda = 288 \text{ nm}$ (Valeur and Weber, 1977), a global rotational correlation time $\theta = 1 \text{ ns}$ is obtained. These results facilitate the determination of the expected anisotropies for the higher concentrations (3% and 7%); they are $\langle r \rangle = 0.090$, and $\langle r \rangle = 0.094$, respectively. As can be seen, they are very close to the experimentally determined ones (Table 1), i.e., the decrease in fluorescence lifetime does not imply a significant variation of anisotropy. This is certainly related to the significant contribution of the limiting anisotropy to the total anisotropy.

From the invariance of anisotropy with concentration it can safely be concluded that there is no significant intermolecular energy migration. For the energy migration in a bi-dimensional system such as a membrane, Snyder and Freire (1982), from Monte Carlo simulations, obtained a decrease in anisotropy for a random distribution of fluorophores in a membrane—and although this was derived for an isotropic rotor, it is relevant to compare these expectations with our data. Considering the Förster radius, $R_0 = 8.5 \text{ \AA}$, as described above (but now calculated from a lower quantum yield, reflected in an also lower lifetime-weighted quantum yield, Table 1), and using the data from Fig. 9 in their work, it can be concluded that for the highest concentration of γM4 studied here (7%, which corresponds to 0.22 molecules within a circle of radius R_0), the reduction in anisotropy should be at most 15%, in full agreement with our data.

From the self-quenching experiments, it was concluded that peptide-rich patches occur, at least in the *lo* phase. Because no energy migration is operative, and due to the small Förster radius for migration, we can obtain structural information about these patches. The absence of energy migration implies that: 1), there is no molecular contact of Trp residues in one dimer with those of another dimer. This indicates that no linear aggregates are formed (Fig. 5 B). If this type of dimer-dimer contact did occur, a strong decrease in anisotropy such as, for example, observed for DHE (Loura and Prieto, 1997) would take place. 2), The formation of dimer “parallel” aggregates cannot be discarded (Fig. 5 C). For this geometry, an inter-Trp minimum distance of 10 Å could be expected. The anisotropy would drop to 78% of its initial value (Eq. 7), and if a small enough fraction of these aggregates were formed, this would not entail a high global migration efficiency. It should be stressed that as stated above for the intramolecular process, there would be no transfer for the other two Trp residues. Moreover, antiparallel interhelical contacts (Fig. 5 D) would not lead to depolarization because the Trp residues would be too far apart, i.e., they would be separated by at least the hydrophobic thickness of the bilayer. The method employed in this work to obtain peptide-containing vesicles cannot discard the occurrence of both possible peptide orientations in the bilayer. It is known, however, that antiparallel contacts are more probable due to stabilization by the opposite sign macrodipole moment in the antiparallel helix (Bowie, 1997) and in *lo*, with a larger hydrophobic thickness, less of the helix termini should protrude to the solvent, thus decreasing solvent screening and increasing the strength of the dipole-dipole interaction relative to *ld*. This can allow for other types of helix-helix interactions like close packing (note that at the extreme of the hydrophobic helix opposite to the Trp⁴⁵³ side, there is a threonine (Thr⁴⁶⁹) and a glycine residue (Gly⁴⁷⁰), both with small side chains that should favor helix approximation, in addition to Gly⁴⁶² and Thr⁴⁶³, approximately in the middle of the γ M4 helix).

Theoretical studies (Ben-Tal and Honig, 1996; Lague et al., 2000) show that under conditions close to those of the present work, interactions between helices in the *ld* phase are either repulsive or require specific interactions, in agreement with the current lack of aggregation of the γ M4 peptide in *ld*. This is in contrast with the experimental study of Yano et al. (2002), in which a 20-mer helix with no specific interactions formed antiparallel dimers at concentrations <1 mol % peptide, and dipole-dipole type stabilizing interactions were invoked.

If the γ M4 peptide formed linear aggregates, there would be no significant interhelix stabilization. This effect would be maximal for the case of antiparallel dimers. However, there would be no need to invoke such a limiting situation if long-range interactions were operative. As shown in Fig. 5 E, patches could be formed with no direct molecular contact, i.e., a small number of lipid molecules would occur in

between the peptides. The helix would induce a local disordering on the acyl chains, together with bilayer deformation, to better match with the hydrophobic portion of the peptides. Once the bilayer was deformed, with an energetic penalty (Lundbaek et al., 2003), other helices would also be better accommodated nearby, justifying the formation of peptide-enriched patches. Patches with an increased local peptide concentration would, in turn, favor the occurrence of dimers.

Relevance to other studies on the AChR

Two basic observations stem from the present work:

1. In a pure POPC system in the *ld* phase, the lipid-protein interactions predominate over interactions between helices, and the γ M4 peptide occurs as an isolated peptide, matching the hydrophobic region of the bilayer.
2. In contrast, in a mixed 60% POPC-40% Chol system in the *lo* phase, peptide-peptide interactions prevail, and peptide aggregation occurs.

These properties of a representative membrane-embedded segment of the AChR may bear relevance to the organization of the γ -subunit α -helical bundle motif and the AChR membrane-spanning region at large. The tendency of the hydrophobic γ M4 peptide to maximize peptide-peptide interactions in the presence but not in the absence of Chol may be related to the ability of this sterol to stabilize the α -helix content of the native AChR (Fong and McNamee, 1987; Butler and McNamee, 1993) and to the inability of reconstituted AChR to respond to agonist stimulation with a cation flux in the absence of Chol (Rankin et al., 1997).

APPENDIX

Sterol segregation in a one-phase system

DHE, the probe used to mimic Chol, has no bulky fluorophores in its structure, thus lacking the disadvantages of other Chol analogs, which were shown to be excluded from Chol-rich phases (Loura et al., 2001a). At the Chol concentration at which the FRET study was carried out (40 mol %), the system is largely in the *lo* phase (Mateo et al., 1995 and de Almeida et al., 2003). The complexity of studying FRET in a biphasic system (Loura, et al., 2001b) is therefore circumvented. The typical radius for an SUV (~25–50 nm) is $\geq 1.5 R_0$, and the system can be safely assumed as being planar with respect to FRET (Eisinger et al., 1981).

The theoretical expectation for a random distribution of acceptors (Fig. 4) involves consideration of the following structural features:

1. The peptide helix was approximated to a cylinder with 10 Å diameter (Bowie, 1997), with the donor located at the axis.
2. The peptide was allowed to incorporate into the bilayer in either direction, i.e., the Trp⁴⁵³ donor can be located close to any of the two membrane/water interfaces, and DHE can in turn be located on either leaflet.

Because R_0 is not small with respect to the membrane thickness, both in-plane and out-of-plane transfer to acceptors in the other membrane leaflet were considered. The experimentally determined values of FRET efficiency,

E , were significantly lower than expected, and the data could only be rationalized with an effective sterol concentration $\sim 38\%$ lower than the analytical expected concentration (see Fig. 4). This does not necessarily mean that there is a tendency to exclude the sterol away from the $\gamma M4$ peptide vicinity, but the area available for the dispersion of sterol is probably reduced because of the formation of peptide-rich patches. This estimated area reduction can, in turn, be compared with that derived from the above-mentioned self-quenching data. The same degree of quenching is obtained for 7 mol % peptide in ld and for all concentrations in lo . Since the diffusion coefficient in lo is threefold lower than in ld (e.g., Dietrich et al., 2001), it can be assumed that the effective concentration of peptide is threefold higher in the patches. Using the area per lipid molecule for the lo phase (see last paragraph) it can be concluded that the $\gamma M4$ peptide occupies $\sim 30\%$ of the area in the patches in agreement with the FRET data.

For the in-plane FRET, Wolber and Hudson (1979) derived the decay of donor fluorescence in the presence of acceptor, assuming a radius of exclusion of acceptors (R_e) around the donor, and a random distribution in the plane of the membrane considered as infinite,

$$\rho_{cis}(t) = \exp \left\{ -\pi R_0^2 n \gamma \left[\frac{2}{3}, \left(\frac{R_0}{R_e} \right)^6 \left(\frac{t}{\langle \tau \rangle} \right) \right] \left(\frac{t}{\langle \tau \rangle} \right)^{1/3} + \pi R_e^2 n \left(1 - \exp \left[-\left(\frac{R_0}{R_e} \right)^6 \left(\frac{t}{\langle \tau \rangle} \right) \right] \right) \right\}, \quad (A1)$$

where n is the surface density of acceptors and

$$\gamma(x, y) = \int_0^y z^{x-1} \exp(-z) dz \quad (A2)$$

is the incomplete Gamma function.

The donor decay resulting from the transfer to acceptors in the opposing membrane leaflet is given by Davenport et al. (1985), as

$$\rho_{trans}(t) = \exp \left\{ -\frac{2c}{\Gamma(2/3) \times b} \times \int_0^{w/\sqrt{w^2+R_e}} [1 - \exp(-tb^3 \alpha^6)] \alpha^{-3} d\alpha \right\}, \quad (A3)$$

where

$$c = \Gamma(2/3) \times n \times \pi \times R_0^2 \times \langle \tau \rangle^{-1/3}. \quad (A4)$$

In this equation, Γ is the complete gamma function, $b = (R_0/w)^2/\langle \tau \rangle^{1/3}$, and w is the interplanar donor-acceptor distance. This value was fixed as $w = 22 \text{ \AA}$ on the basis of molecular models.

The FRET efficiency E is finally computed numerically by

$$E = 1 - \frac{\int_0^\infty i_D(t) \rho_{cis}(t) \rho_{trans}(t) dt}{\langle \tau \rangle_D}, \quad (A5)$$

which corresponds to Eq. 5.

In the calculation of the surface density of acceptors, the condensing effect of Chol on the lipid surface was considered ($\sim 7 \text{ \AA}^2/\text{molecule}$; Smaby et al., 1997), together with an area/molecule of 66.4 \AA^2 for POPC (Chiu et al., 1999) and 37.7 \AA^2 for Chol (Smaby et al., 1997).

We thank Fundação para a Ciência e a Tecnologia, Portugal, for financing research projects and R.F.M.A.'s PhD grant (SFRH/BD/943/2000) under the program POCTI.

This work was supported in part by grants from the Universidad Nacional del Sur, the Agencia Nacional de Promoción Científica (FONCYT),

Argentina, and Fogarty International Research Collaboration Award 1-RO3-TW01225-01 (National Institutes of Health) to F.J.B., and a grant from the Biotechnological and Biological Science Research Council (UK) to A.W.

REFERENCES

- Addona, G. H., H., Sandermann, M. A. Kloczewiak, S. S. Husain, and K. W. Miller. 1998. Where does cholesterol act during activation of the nicotinic acetylcholine receptor? *Biochim. Biophys. Acta.* 1370: 299–309.
- Antollini, S. S., and F. J. Barrantes. 1998. Disclosure of discrete sites for phospholipid and sterols at the protein-lipid interface in native acetylcholine receptor-rich membrane. *Biochemistry.* 37:16653–16662.
- Antollini, S. S., and F. J. Barrantes. 2002. Unique effects of different fatty acid species on the physical properties of the *Torpedo* acetylcholine receptor membrane. *J. Biol. Chem.* 277:1249–1254.
- Baenziger, J. E., M. L. Morris, T. E. Darsaut, and S. E. Ryan. 2000. Effect of membrane lipid composition on the conformational equilibria of the nicotinic acetylcholine receptor. *J. Biol. Chem.* 275:777–784.
- Barrantes, F. J. 1998. The Nicotinic Acetylcholine Receptor: Current Views and Future Trends. Springer-Verlag, Berlin/Heidelberg, and Landes Publishing, Georgetown, TX.
- Barrantes, F. J. 2001. Fluorescence studies of the acetylcholine receptor: structure and dynamics in the membrane environment. *J. Fluorescence.* 11:273–285.
- Barrantes, F. J. 2003. Transmembrane modulation of nicotinic acetylcholine receptor function. *Curr. Opin. Drug Disc. Develop.* 6:620–632.
- Barrantes, F. J., S. S. Antollini, M. P. Blanton, and M. Prieto. 2000. Topography of nicotinic acetylcholine receptor membrane-embedded domains. *J. Biol. Chem.* 275:37333–37339.
- Berberan-Santos, M. N., and M. Prieto. 1987. Energy transfer in spherical geometry. Application to micelles. *J. Chem. Soc. Faraday Trans. 2.* 83:1391–1407.
- Ben-Tal, N., and B. Honig. 1996. Helix-helix interactions in lipid bilayers. *Biophys. J.* 71:3046–3050.
- Berberan-Santos, M. N., and B. Valeur. 1991. Fluorescence depolarization by electronic energy transfer in donor-acceptor pairs of like and unlike chromophores. *J. Chem. Phys.* 95:8048–8055.
- Blanton, M. P., and J. B. Cohen. 1992. Mapping the lipid-exposed regions in the *Torpedo californica* nicotinic acetylcholine receptor. *Biochemistry.* 31:3738–3750.
- Blanton, M. P., and J. B. Cohen. 1994. Identifying the lipid-protein interface of the *Torpedo* nicotinic acetylcholine receptor: secondary structure implications. *Biochemistry.* 33:2859–2872.
- Blanton, M. P., Y. Xie, L. J. Dangott, and J. B. Cohen. 1999. The steroid promegestone is a noncompetitive antagonist of the *Torpedo* nicotinic acetylcholine receptor that interacts with the lipid-protein interface. *Mol. Pharmacol.* 55:269–278.
- Blanton, M. P., and H. H. Wang. 1991. Localization of regions of the *Torpedo californica* nicotinic acetylcholine receptor labeled with an aryl azide derivative of phosphatidylserine. *Biochim. Biophys. Acta.* 1067:1–8.
- Bowie, J. U. 1997. Helix packing in membrane proteins. *J. Mol. Biol.* 272:780–789.
- Butler, D. H., and M. G. McNamee. 1993. FTIR analysis of nicotinic acetylcholine receptor secondary structure in reconstituted membranes. *Biochim. Biophys. Acta.* 1150:17–24.
- Castanho, M. A. R. B., N. C. Santos, and L. M. S. Loura. 1997. Separating the turbidity spectra of vesicles from the absorption spectra of membrane probes and other chromophores. *Eur. Biophys. J.* 26:253–259.
- Chattopadhyay, A., and M. G. McNamee. 1991. Average membrane penetration depth of tryptophan residues of the nicotinic acetylcholine receptor by the parallax method. *Biochemistry.* 30:7159–7164.

- Chen, R. F. 1967. Fluorescence quantum yields of tryptophan and tyrosine. *Analyt. Lett.* 1:35–42.
- Chen, Y., and M. D. Barkley. 1998. Toward understanding tryptophan fluorescence in proteins. *Biochemistry*. 37:9976–9982.
- Chiu, S.-W., E. Jakobsson, S. Subramaniam, and H. L. Scott. 1999. Combined Monte Carlo and molecular dynamics simulation of fully hydrated dioleoyl and palmitoyl-oleoyl phosphatidylcholine lipid bilayers. *Biophys. J.* 77:2462–2469.
- Corbin, J., N. Méthot, H. H. Wang, J. E. Baenziger, and M. P. Blanton. 1998. Secondary structure analysis of individual transmembrane segments of the nicotinic acetylcholine receptor by circular dichroism and Fourier transform infrared spectroscopy. *J. Biol. Chem.* 273:771–777.
- Criado, M., W. L. C. Vaz, F. J. Barrantes, and T. M. Jovin. 1982. Translational diffusion of acetylcholine receptor (monomeric and dimeric forms) of *Torpedo marmorata* studied by fluorescence recovery after photobleaching. *Biochemistry*. 21:5750–5755.
- Davenport, L., R. E. Dale, R. B. Bisby, and R. B. Cundall. 1985. Transverse location of the fluorescent probe 1,6-diphenyl-1,3,5-hexatriene in model lipid bilayer membrane systems by resonance excitation energy transfer. *Biochemistry*. 24:4097–4108.
- de Almeida, R. F. M., L. M. S. Loura, A. Fedorov, and M. Prieto. 2002. Non-equilibrium phenomena in the phase separation of a two-component lipid bilayer. *Biophys. J.* 82:823–834.
- de Almeida, R. F. M., A. Fedorov, and M. Prieto. 2003. Sphingomyelin/phosphatidylcholine/cholesterol phase diagram: boundaries and composition of lipid rafts. *Biophys. J.* 85:2406–2416.
- Deeg, R., and J. Ziegenhorn. 1983. Kinetic enzymic method for automated determination of total cholesterol in serum. *Clin. Chem.* 29:1798–1802.
- Dietrich, C., L. A. Bagatolli, Z. Volovyk, N. L. Thompson, M. Levi, K. Jacobson, and E. Gratton. 2001. Lipid rafts reconstituted in model membrane systems. *Biophys. J.* 80:1417–1428.
- Eisinger, J., W. E. Blumberg, and R. E. Dale. 1981. Orientational effect in intra- and intermolecular long range excitation energy transfer. *Ann. N. Y. Acad. Sci.* 366:155–175.
- Fong, T. M., and M. G. McNamee. 1987. Stabilization of acetylcholine receptor secondary structure by cholesterol and negatively charged phospholipids in membranes. *Biochemistry*. 26:3871–3880.
- Gill, S. C., and P. H. von Hippel. 1989. Calculation of protein extinction coefficients from amino acid sequence data. *Analyt. Biochem.* 182:319–326.
- Ipsen, J. H., G. Karlström, O. G. Mouritsen, H. Wennerström, and M. J. Zuckermann. 1987. Phase equilibria in the phosphatidylcholine-cholesterol system. *Biochim. Biophys. Acta.* 905:162–172.
- Jones, O. T., and M. G. McNamee. 1988. Annular and nonannular binding sites for cholesterol associated with the nicotinic acetylcholine receptor. *Biochemistry*. 27:2364–2374.
- Lague, P., M. J. Zuckermann, and B. Roux. 2000. Lipid-mediated interactions between intrinsic membrane proteins: a theoretical study based on integral equations. *Biophys. J.* 79:2867–2879.
- Lakowicz, J. R. 1999. Principles of Fluorescence Spectroscopy, 2nd Ed. Kluwer Academic/Plenum Publishers, New York, NY.
- Loura, L. M. S., A. Fedorov, and M. Prieto. 1996. Resonance energy transfer in a model system of membranes: application to gel and liquid crystalline phases. *Biophys. J.* 71:1823–1836.
- Loura, L. M. S., and M. Prieto. 1997. Dehydroergosterol structural organization in aqueous medium and in a model system of membranes. *Biophys. J.* 72:2226–2236.
- Loura, L. M. S., A. Fedorov, and M. Prieto. 2001a. Exclusion of a cholesterol analog from the cholesterol-rich phase in model membranes. *Biochim. Biophys. Acta.* 1511:236–243.
- Loura, L. M. S., R. F. M. de Almeida, and M. Prieto. 2001b. Detection and characterization of membrane microheterogeneity by resonance energy transfer. *J. Fluorescence.* 11:197–209.
- Lundbaek, J. A., O. S. Anderson, T. Werge, and C. Nielsen. 2003. Cholesterol-induced protein sorting: an analysis of energetic feasibility. *Biophys. J.* 84:2080–2089.
- Marquardt, D. W. 1963. An algorithm for least-squares estimation of non-linear parameters. *J. Soc. Ind. Appl. Math.* 11:431–441.
- Marsh, D., and F. J. Barrantes. 1978. Immobilized lipid in acetylcholine receptor-rich membranes from *Torpedo marmorata*. *Proc. Natl. Acad. Sci. USA.* 75:4329–4333.
- Marsh, D. A. Watts, and F. J. Barrantes. 1981. Phospholipid chain immobilization and steroid rotational immobilization in acetylcholine receptor-rich membranes from *Torpedo marmorata*. *Biochim. Biophys. Acta.* 645:97–101.
- Mateo, C. R., A. U. Acuña, and J.-C. Brochon. 1995. Liquid-crystalline phases of cholesterol/lipid bilayers as revealed by the fluorescence of *trans*-parinaric acid. *Biophys. J.* 68:978–987.
- McClare, C. W. 1971. An accurate and convenient organic phosphorus assay. *Analyt. Biochem.* 39:527–530.
- Méthot, N., B. D. Ritchie, M. P. Blanton, and J. E. Baenziger. 2001. Structure of the pore-forming transmembrane domain of a ligand-gated ion channel. *J. Biol. Chem.* 276:23726–23732.
- Miyazawa, A., Y. Fujiyoshi, and N. Unwin. 2003. Structure and gating mechanism of the acetylcholine receptor pore. *Nature.* 423:949–955.
- Owen, C. S. 1975. Two-dimensional diffusion theory: cylindrical diffusion model applied to fluorescence quenching. *J. Chem. Phys.* 62:3204–3207.
- Rankin, S. E., G. H. Addona, M. A. Kloczewiak, B. Bugge, and K. W. Miller. 1997. The cholesterol dependence of activation and fast desensitization of the nicotinic acetylcholine receptor. *Biophys. J.* 73:2446–2455.
- Razi-Naqvi, K. 1974. Diffusion-controlled reactions in two dimensional fluids: discussion of measurements of lateral diffusion of lipids in biological membranes. *Chem. Phys. Lett.* 28:2303–2304.
- Ridder, A. N. J. A., S. Morein, J. G. Stam, A. Kuhn, B. de Kruijff, and J. A. Killian. 2000. Analysis of the role of interfacial tryptophan residues in controlling the topology of membrane proteins. *Biochemistry.* 39:6521–6528.
- Runnels, L. W., and S. F. Scarlata. 1995. Theory and application of fluorescence homotransfer to melittin oligomerization. *Biophys. J.* 69:1569–1583.
- Santos, N. C., M. Prieto, and M. A. R. B. Castanho. 1998. Interaction of the major epitope region of HIV protein gp41 with membrane model systems. A fluorescence spectroscopy study. *Biochemistry.* 37:8674–8682.
- Sillen, A., and Y. Engelborghs. 1998. The correct use of “average” fluorescence parameters. *Photochem. Photobiol.* 67:475–486.
- Sklar, L. A., B. S. Hudson, M. Petersen, and J. Diamond. 1977. Conjugated polyene fatty acids on fluorescent probes: spectroscopic characterization. *Biochemistry.* 16:813–819.
- Smaby, J. M., M. M. Momsen, H. L. Brockman, and R. E. Brown. 1997. Phosphatidylcholine acyl unsaturation modulates the decrease in interfacial elasticity induced by cholesterol. *Biophys. J.* 73:1492–1505.
- Small, D. M. 1986. The Physical Chemistry of Lipids, Handbook of Lipid Research, Vol. 4. Plenum Press, New York, NY.
- Smutzer, G., B. F. Crawford, and P. L. Yeagle. 1986. Physical properties of the fluorescent sterol probe dehydroergosterol. *Biochim. Biophys. Acta.* 862:361–371.
- Snyder, B., and E. Freire. 1982. Fluorescence energy transfer in two dimensions. A numeric solution for random and non-random distributions. *Biophys. J.* 40:137–148.
- Szabo, A. G., and D. M. Rayner. 1980. The time-resolved emission spectra of peptide conformers measured by pulsed laser excitation. *Biochem. Biophys. Res. Commun.* 94:909–915.
- Umberger, J. Q., and V. K. Lamer. 1945. The kinetics of diffusion controlled molecular and ionic reactions in solution as determined by measurements of the quenching of fluorescence. *J. Am. Chem. Soc.* 67:1099–1109.
- Valeur, B., and G. Weber. 1977. Resolution of the fluorescence excitation spectrum of indole into the 1L_a and 1L_b excitation bands. *Photochem. Photobiol.* 25:441–444.

- Valeur, B. 2001. *Molecular Fluorescence. Principles and Applications*. Wiley-VCH, New York, NY.
- Van Der Meer, B., G. Coker III, and S.-Y. S. Chen. 1994. *Resonance Energy Transfer: Theory and Data*. VCH Publishers, New York, NY.
- Vaz, W. L. C., M. Criado, V. M. C. Madeira, G. Schoellmann, and T. M. Jovin. 1982. Size dependence of the translational diffusion of large integral membrane proteins in liquid-crystalline phase lipid bilayers. A study using fluorescence recovery after photobleaching. *Biochemistry*. 21:5608–5612.
- Vierl, U., L. Löbbecke, N. Nagel, and G. Cevc. 1994. Solute effects on the colloidal and phase behavior of lipid bilayer membranes: ethanol-dipalmitoylphosphatidylcholine mixtures. *Biophys. J.* 67:1067–1079.
- Vogel, H., L. Nilsson, R. Rigler, K.-L. Vogues, and G. Jung. 1988. Structural fluctuations of a helical polypeptide traversing a lipid bilayer. *Proc. Natl. Acad. Sci. USA*. 85:5067–5071.
- Wiener, M. C., and S. H. White. 1992. Structure of a fluid dioleoyl-phosphatidylcholine bilayer determined by joint refinement of x-ray and neutron diffraction data. III. Complete structure. *Biophys. J.* 61: 437–447.
- Wolber, P. K., and B. S. Hudson. 1979. An analytic solution to the Förster energy transfer problem in two dimensions. *Biophys. J.* 28:197–210.
- Yano, Y., T. Takemoto, S. Kobayashi, H. Yasui, H. Sakurai, W. Ohashi, M. Niwa, S. Futaki, Y. Sugiura, and K. Matsuzaki. 2002. Topological stability and self-association of a completely hydrophobic model transmembrane helix in lipid bilayers. *Biochemistry*. 41:3073–3080.
- Zamyatnin, A. A. 1972. Protein volume in solution. *Prog. Biophys. Mol. Biol.* 24:107–123.